AIMS Biophysics, 7(4): 248–266.
DOI: 10.3934/biophy.2020019
Received: 06 May 2020
Accepted: 22 June 2020
Published: 03 July 2020

http://www.aimspress.com/journal/biophysics

Research article

RETRACTED: Thermal investigation of montmorillonite/BSA by Fourier Transform InfraRed Spectroscopy measurements

Maria Teresa Caccamo[1,*], Giuseppe Mavilia[1], Letterio Mavilia[2], Pietro Calandra[3], Domenico Lombardo[4] and Salvatore Magazù[1]

[1] Dipartimento di Scienze Matematiche e Informatiche, Scienze Fisiche e Scienze della Terra, Università di Messina, Viale Ferdinando Stagno D'Alcontres n. 31, S. Agata, 98166 Messina, Italy
[2] Dipartimento di Patrimonio, Architettura e Urbanistica; Università Mediterranea di Reggio Calabria, (PAU), Via Melissari, I - 89124 Reggio Calabria, Italy
[3] Consiglio Nazionale delle Ricerche, Istituto per lo Studio Materiali Nanostrutturati, Via Salaria Km 29,300 00015 Monterotondo Stazione (Roma), Italy
[4] CNR–IPCF, Istituto per i Processi Chimico Fisici – (Sez. Messina) Viale F. Stagno D'Alcontres, 37. I-98158, Messina, Italy

*** Correspondence:** Email: mtcaccamo@unime.it; Tel: +390906765019.

Abstract: This paper reports the analysis of the intramolecular OH stretching band obtained by Fourier Transform Infrared (FTIR) spectroscopy measurements. In order to characterize the effect of montmorillonite on the properties of Bovine Serum Albumin (BSA) the two-state model is adopted for the analysis of the OH stretching band. We assume that the OH stretching can be divided into two different states of inter-molecular bonding. The results of this experimental work confirm that the montmorillonite leads to a stabilization of the BSA structure. Also, the analysis of the spectra temperature dependence shows a montmorillonite-induced higher thermal stability of the BSA in respect to pristine BSA. Thus, this paper allows to highlight the importance of montmorillonite as thermal bio-protector: this is also evidenced by the theory widely discussed in the following introduction regarding the birth of the first life forms on earth in montmorillonite clay, in which the protective role of the montmorillonite interlayer space is also highlighted. A FTIR analysis was carried out to investigate the interaction of montmorillonite with BSA. Two different approaches, i.e. Spectral Distance and Wavelet analyses, constitute two effective and innovative approaches for the characterization of the thermal properties of pristine BSA and of BSA in the presence of montmorillonite. The results allowed us to consider as BSA in the presence of montmorillonite has a lower spectral sensitivity when the temperature changes and, therefore, the role of montmorillonite

as a thermal bio-protector is motivated.

Keywords: bovine serum albumin, montmorillonite, Fourier Transform InfraRed Spectroscopy

1. Introduction

Many theories have been proposed on the origins of life on earth: in the Russian book of 1924, Oparin hypothesized that simple molecules (CH_4, NH_3) reacted to form small bio-molecules and bio-polymers (nucleotides, peptides,). They, then, evolve in multimolecular systems and, finally, they gave rise to the first forms of life [1]. Later, in a book of 1929, Haldane proposed a similar theory about the origins of life [2]: but, it was Bernal (1951) that suggested that clays had a fundamental role in chemical evolution and in the origins of life due to their ability to absorb, protect from ultraviolet radiation and catalyze the polymerization of organic molecules [3]. Then, Cains-Smith (1982) has proposed that clays can act as genetic candidates [4]. Hence, the inclusion of organic molecules and monomers in the layered structure of clays, such as montmorillonite and kaolinite, would favor the formation and replication of biopolymers such as enzymes and polynucleotides. In this introduction, we present a summary of data relating to different studies present in the literature to show as montmorillonite could be considered the cradle of the evolution of the early life forms on earth and, also, we want to highlight the role of the mal bio-protector of the montmorillonite clay. We propose, in fact, that the birth of life occurs on clays and in particular in montmorillonite [5–12]. Considering RNA as the fundamental component of primordial life characterized by catalytic and genetic properties, some theoretical steps are described below which show as the formation of RNA precursors would occur in the montmorillonite structure. Then, there is the phase related not only to the formation of RNA as oligomers parallel to the sheets in the interlayer spaces, but also to the fixing of some trimers at the edges of the sheets of adjacent layers perpendicular to their surfaces since the length of each individual trimer is equal to the interlayer distance. The encapsulation of each trimer with an oligomer attracted to a fatty acid-composed vesicle would be the starting point for the formation of a codon-anticodon complex which could determine to the birth of a primordial genetic code [13–18]. The interaction between water, heat and rock gave rise to the first forms of life: water, in fact, is an indispensable element for any form of life and, in fact, many chemicals dissolve easily in the water and, therefore, could be mixed and give rise to chemical reactions [20–21]. We assume that the evolution of the first life forms would have occurred within the earth's surface and more precisely on the rock constituted from clay-rich soil layers. In fact, in the presence of water, montmorillonite clay can form a filter and allow the soil layers to become impermeable [22–25]. There are three main groups of clay such as kaolinite, illite and smectite: the most common smectite is montmorillonite, which is the main constituent of bentonite, derived by volcanic ash, and it is very likely that it was present in the earth's crust in its primitive state. Based on the number and arrangement of the tetrahedral and octahedral sheets contained in the layers of crystal structure, silicate-based clays are classified into two different groups: minerals of type 1: 1 (a tetrahedral and an octahedral sheet) and type 2: 1 minerals [26–29]. Therefore, there are two types of phyllosilicates: those with a 1: 1 ratio, such as kaolinite, in which each lamella is formed by only two layers (one octahedral and one tetrahedral) and the phyllosilicates with a 2: 1 ratio, such as montmorillonite, in which a single layer is formed by an octahedral sheet interposed between two tetrahedral sheets and,

moreover, there is the presence of weak Van der Waals bonds between the various layers [30–35]. Figure 1 schematically shows the schematic structure of montmorillonite.

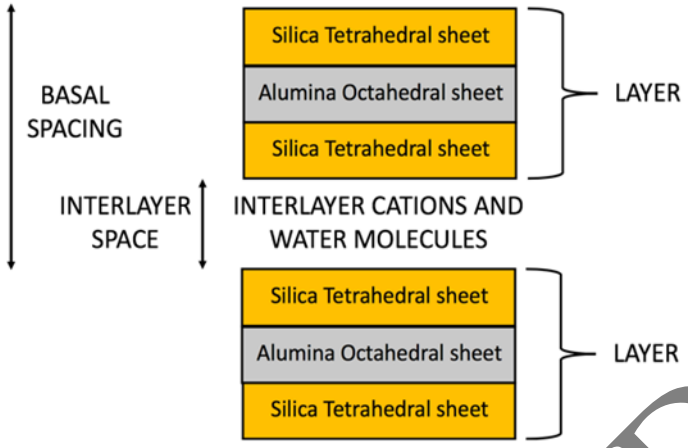

Figure 1. Schematic structure of montmorillonite with a 2:1 ratio, in which each layer consists by two silica tetrahedral sheets with an interposed alumina octahedral sheet.

The montmorillonite formula is $(Al^{0.2}Si^{7.8})^{IV}(Mg^{0.6}Al^{3.4})^{VI}O_{20}(OH)_4$: its composition, without considering the presence of the material between the various layers, is: Al_2O_3 (28,3%), SiO_2 (66,7%), H_2O (5%), which allows us to show as in the montmorillonite there may be isomorphic substitutions of the Si^{4+} cations with Al^{3+} within the tetrahedral sheets, and of the Al^{3+} cation with Mg^{2+} in the octahedral sheets. So, the montmorillonite charge for each layer is: [7.8 (+4)] + [0.2 (+3)] + [3.4 (+3)] + [0.6 (+2)] + [20 (−2)] + [4 (−1)] = −0.8 charge/unit cell. So, these layers are characterized by an excess negative charge, which is balanced by the elements in the interlayer spaces such as alkaline or alkaline-earth cations, solvated in turn by water molecules. Due to this peculiar structure, montmorillonite has many physicochemical properties such as a large surface area, high adsorption capacity, swelling and ion exchange [36–39]. Moreover, the interlayer space of montmorillonite depends on the degree of hydration of the mineral: by increasing the number of water layers, the crystalline lattice expands (Figure 2); by complete dehydration, however, it loses its ability to expand. In fact, in the presence of water, H_2O molecules dispose themselves within the montmorillonite interlayer space, generating an increased space between the layers.

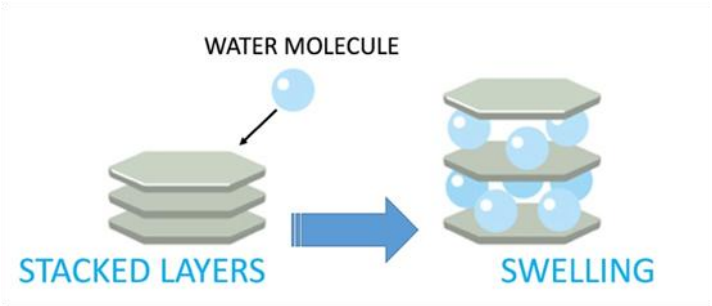

Figure 2. Swelling of montmorillonite clay in water.

Regarding the water absorption capacity, this property is very important for these clays. In fact, clays can absorb or desorb water as a function of changes in the moisture content: as above reported, when H_2O molecules are absorbed, they fill the space between the various layers. Montmorillonite has excellent water absorption properties; however, the interaction between the water molecules and montmorillonite can produce swelling. The absorption of water molecules and the swelling of montmorillonite determine to the formation of hydrated states and can give rose to hysteresis phenomena. The montmorillonite swelling and hydration processes play a fundamental role for a wide variety of engineering applications. Furthermore, the anisotropy of a wide class of clays is reflected in a broad variable range of mechanical properties. The structure of hydrated montmorillonite is shown in Figure 2: this anisotropy of montmorillonite can produce great differences in the values of elastic constants, shear modulus, and Young's modulus. Moreover, these mechanical properties decrease with increasing hydration [40–42]. Furthermore, as regards the thermal properties, montmorillonite is a good thermal insulator and, moreover, it allows to increase the thermal stability once added as an additive in many materials. Recent developments in the use of self-assembling supramolecular objects to fabricate innovative well-defined nanomaterials links soft matter chemistry to hard matter sciences [43–46] and requires the employment of techniques and approaches that to simultaneously detect the structure re-organization and dynamics at the nanoscale [47–49]. This is a significant area of research to produce thermal barrier effects in the structure of the composite material: in fact, the thermal barrier properties of clays are appreciated in many applications involving the use of heat-resistant materials and flame retardants. The nanoclays have been largely studied and used in polymer matrix composites to obtain greater thermal stability and better flame retardancy properties. The variation of thermal expansion, under the effect of heat, for metals, polymers and ceramics was analyzed: generally, the order of magnitude of the thermal expansion in polymers, metals and ceramics can be indicated as follows: polymer> metal> ceramics. This order is based on the values of the linear thermal expansion coefficient in the values range 20–100, 3–20 and 3–5 ppm/℃ for polymers, metals and ceramics, respectively [50]. Therefore, a higher thermal stability of montmorillonite allows its use as a filler in polymers to make composite materials with a low coefficient of thermal expansion. However, the improvement of the thermal stability of the polymers requires an increase in the ratio between surface and volume of a material (aspect ratio) and, therefore, can be obtained for values of this aspect ratio higher than 100. Many experimental studies have been conducted to explain the fundamental role played by ribonucleic acid (RNA) in the evolution of early life forms. The three main steps that would lead to the formation of the first life forms with the birth of a primordial genetic code are summarized below. Montmorillonite can catalyze the formation of RNA oligomers in aqueous solution through the union of RNA nucleotides, which in turn join together to form longer chains [51]. The extent of this catalysis depends on the value of the negative charge present inside the montmorillonite and on the number of cations associated with it. Under certain experimental conditions, it is possible to obtain oligomers of 40 to 50-mers up to the length of small ribozymes [52–54]. As reported previously, the surfaces of the montmorillonite layers have a negative charge: in wet conditions, the quantity of water and cations present in the environment allow a variable space between the layers occupied by water and cations. While, in dry conditions, these interlayer spaces are reduced and occupied by hydrated cations, which hold together the layers. Therefore, montmorillonite is able to expand and contract its structures maintaining its crystallographic integrity. Due to this ability, the oligomerization of RNA nucleotides would occur mainly in the interlayer space parallel to the surface sheets of

montmorillonite [55–58] (Figure 3). Consequently, for a development of the oligomerization process of RNA nucleotides in the interlayer space of montmorillonite, we propose that it is moderately expanded, i.e. in the presence of low quantities of water and cations [59–62] (Figure 3).

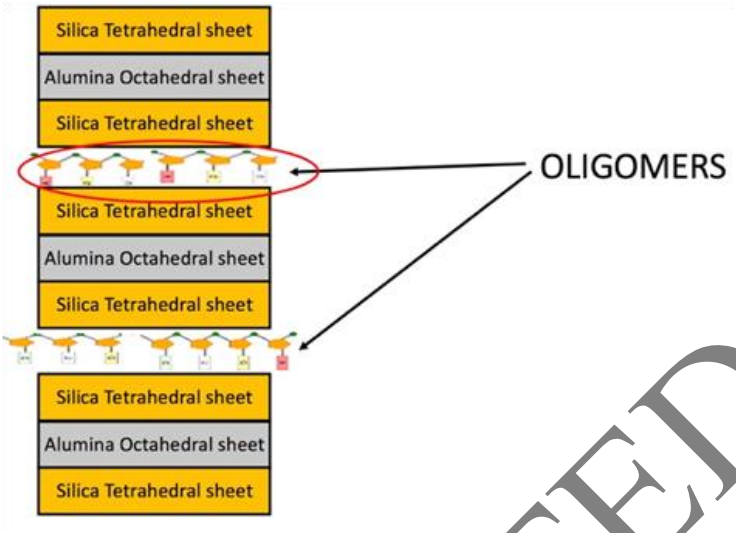

Figure 3. Schematic representation of the formation of RNA oligomers in the interlayer space in presence of low number of cations and water molecules.

As reported previously, the formation of numerous RNA oligomers occurred in the space between the parallel layers to the montmorillonite sheets in the presence of a low amount of water. During the rainy period, the water with the cations diffuses inside the interlayer space until it reaches a size of 1.02 nm (Figure 4). Consequently, the RNA oligomers leave the interlayer space under the pressure of the water and the cations: after this exit, some trimers, positioned perpendicular to the sheets of the adjacent layers, react with their two ends the edge of these sheets surfaces when the length of the trimers is equal to the interlayer space of 1.02 nm [63–64].

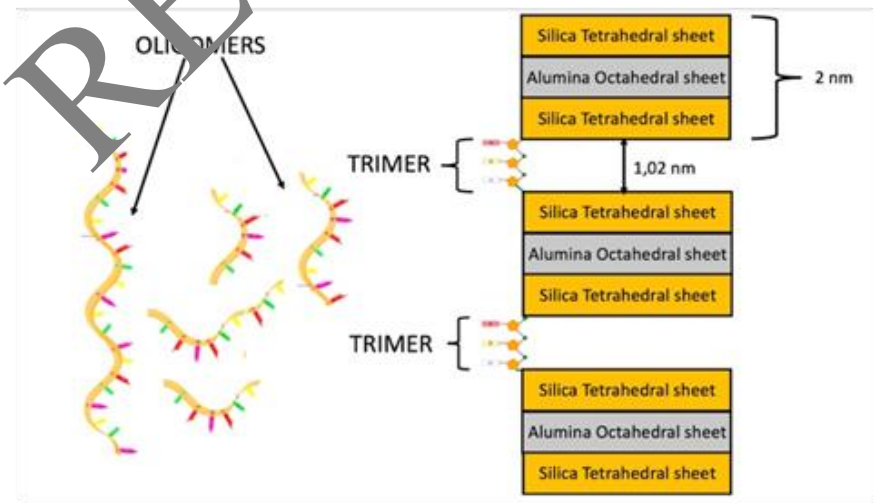

Figure 4. Exit of the oligomers from interlayer space and positioning of trimers in a position perpendicular to the sheets of adjacent layers.

According to this theory, the RNA oligomers are protected by the montmorillonite layers, but, after their exit from the interlayer space, they need protection from some prebiotic conditions such as the high temperature and the high quantities of UV radiation. For this protection, it has been proven that montmorillonite can also catalyze the formation of vesicles composed of simple aliphatic carboxylic acids present in the prebiotic environment and that the clay particles and/or RNA oligomers could encapsulate inside of these vesicles [65–66]. We propose that, in presence of prebiotic conditions, the RNA oligomers can be encapsulated inside fatty acids-composed vesicles, which provide protection and environments for further biochemical reactions (Figure 5). Furthermore, these fatty acids-composed vesicles show permeability to the nucleotides in such a way as to allow the nucleic acid to be stretched within them. They exhibit high thermal stability and keep DNA and RNA oligonucleotides within them at temperatures between 0 ℃ and 100 ℃ [67]. Then, each fixed trimer would be encapsulated with the closest oligomer attracted to a vesicle in which a codon-anticodon complexes might emerge (Figure 5): the accompanying oligomer should evolve in RNA transfer (tRNA) by binding with one of its complementary sequence (anticodon) to the fixed trimer considered as a codon and by the presence of new nucleotides that could enter through the membrane of this vesicle defined as codon-anticodon vesicle. However, each free oligomer would be encapsulated alone or with the others in a vesicle in which these oligomers could increase in length by binding together and/or adding new nucleotides present to produce new possible ribozymes.

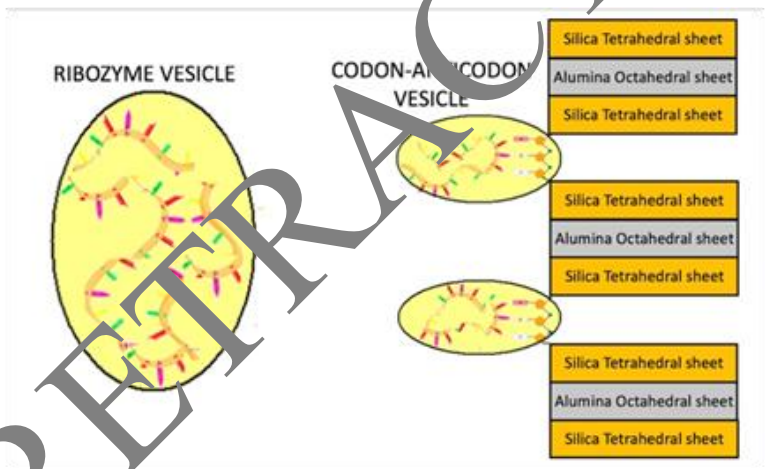

Figure 5. Formation of codon-anticodon complexes in protective vesicles.

After this wet period and at the beginning of a dry period, the amount of water starts to be low and, consequently, the montmorillonite interlayer spaces decrease until reaching the state of a possible resumption of the formation of new RNA oligomers. However, during the reduction of the interlayer space, each codon-anticodon vesicle detaches itself from the edges of the sheets and it is located, outside the crystalline structure of the clay itself, in contact with the vesicle above and below. Hence, these vesicles would merge to allow to the connection between nucleotides of subsequent triplets: as a result, a long chain of codon-anticodon complexes may appear within a long single vesicle. This chain would represent the first operational RNA already connected to the corresponding tRNA. So, in summary, the encapsulation of each fixed trimer with an oligomer attracted to a fatty acids-composed vesicle would be the starting point for the formation of a codon-anticodon complex

which could lead to the birth of a primordial genetic code. The development of advanced nanomaterials exploit the self-assembly process that involves the combination of non-covalent soft interactions with the multi-functionality of building blocks and provides an excellent strategy for the preparation of novel, advanced nanomaterials with highly controlled properties for biotechnology and material science application [68–71]. Previously, it has been highlighted that clays have a high specific surface, cation exchange capacity and absorption capacity and, therefore, they are appreciated for their high absorption capacity of cations including Ag^{+}, Zn^{2+} and Cu^{2+}. Furthermore, previous research in the literature has shown that clays modified with these cations have antibacterial properties [72–77]. As regards, however, the antibacterial properties of montmorillonite modified with Fe^{3+} cations, some studies in the literature have shown effective removal of phenolic organic compounds from wastewater due to the oxidative oligomerization catalyzed on the surface by the same Fe^{3+} saturated montmorillonite [78–80]. Moreover, it has been hypothesized that the Fe^{3+} saturated montmorillonite could also be able to eliminate the bacteria present in the wastewater. Although montmorillonites modified with Cu^{2+}, Zn^{2+} and Ag^{+} cations show antibacterial activity, the presence of these cations in water could pose a potential risk to public health due to their toxicity at high concentrations. Therefore, it was proposed to use the saturated montmorillonite of Fe^{3+} as a possible alternative for the water disinfection process because iron is an essential element for humans [81]. In summary, the effectiveness of Fe^{3+} saturated montmorillonite for the elimination of bacteria present in secondary wastewater has been demonstrated. So, these experimental results suggest as the montmorillonite modified with Fe^{3+} cations could probably be used as an effective antibacterial material for water disinfection in small plants used for the treatment of drinking water and in large plants used for the treatment of drinking water and wastewater. In this experimental work, samples of montmorillonite and its mixture with Bovine Serum Albumin (BSA) were investigated as a function of temperature by means of Fourier Transform Infrared (FTIR) spectroscopy technique and Spectral Distance (SD) approach. In order to determine the thermal protective effects of Montmorillonite on a system of biophysical interest, a protein, the Bovine Serum Albumin (BSA) was chosen [82–89]. It is a serum albumin protein derived from cows and it has numerous biochemical applications such as ELISAs (Enzyme-Linked Immunosorbent Assay) and immunohistochemistry [90–95]. Bovine Serum Albumin (BSA) is a small, soft, stable, non-reactive protein, and it is used as a representative short peptide in the drug delivery system [96–101]. It is well known that exist different techniques to investigate the behaviours of proteins, such as X-rays, Nuclear Resonance Magnetic, Neutron Scattering, Dynamic Light Scattering, Acoustic Levitation, Raman spectroscopy and InfraRed absorption [102–110].

2. Materials and method

Pristine montmorillonite powders purchased from Merck (Milano, Italy, surface area 250 m^2/g), BSA (purchased from Sigma) and double distilled water were used to prepare the samples. Montmorillonite/water mixtures have been prepared by adding to pure protein double-distilled water (80 wt% montmorillonite); for montmorillonite/water/BSA mixtures the concentration was: 80 wt% montmorillonite/20 wt% (BSA (50 wt%)+ H_2O (50 wt%)). Fourier Transform InfraRed (FTIR) spectroscopy allows us to characterize the molecule rotational and vibrational motions. This spectroscopic technique explores 14000–10 cm^{-1} range of the electromagnetic spectrum, which encloses the Near-IR range (14000–4000 cm^{-1}), the Mid-IR range (4000–400 cm^{-1}), and the Far-IR (400–10 cm^{-1}).

FTIR technique is a powerful method to investigate the structural and dynamical properties of materials as well as their dependence on temperature: this technique is based on the analysis of the absorption spectra [111–114]. In this experimental work, we collected vibrational spectra by means of the Vertex 70v spectrometer (Bruker Optics, Ettlingen, Germany) using a Platinum diamond ATR. All spectra were collected by using an average of 96 scans with a resolution of 4 cm^{-1} in a spectral range of 4000~400 cm^{-1}, from a temperature of 20 ℃ to 55 ℃. The pre-processing data procedure was performed through OPUS software and, then, by means of Matlab environment. Due to the complexity of the investigated systems we prefer to analyze globally the spectral features of the samples by applying an innovative approach consisting in the integrated use of the Spectral Distance and Wavelet Cross Correlation protocols. Such an approach reveals to be very effective since in the present study we focus the attention only on the spectra temperature dependence. On this purpose, to characterize the temperature sensitivity of the analyzed samples, the Spectral Distance approach has been used; this latter is based on the following expression:

$$SD = \left(\sum [A(\omega,T) - I(\omega,T_i)]^2 \cdot \Delta\omega\right)^{\frac{1}{2}} \quad (1)$$

where $A(\omega)$ represents the absorbance at the frequency ω, T_i denotes the lowest temperature, that is 20 ℃ and $\Delta\omega$ is the frequency resolution of the instrument.

3. Results and discussion

In Figure 6, the FTIR spectrum of montmorillonite in the spectral range of 4000 ÷ 400 cm^{-1} at the temperature of T = 20 ℃ is reported.

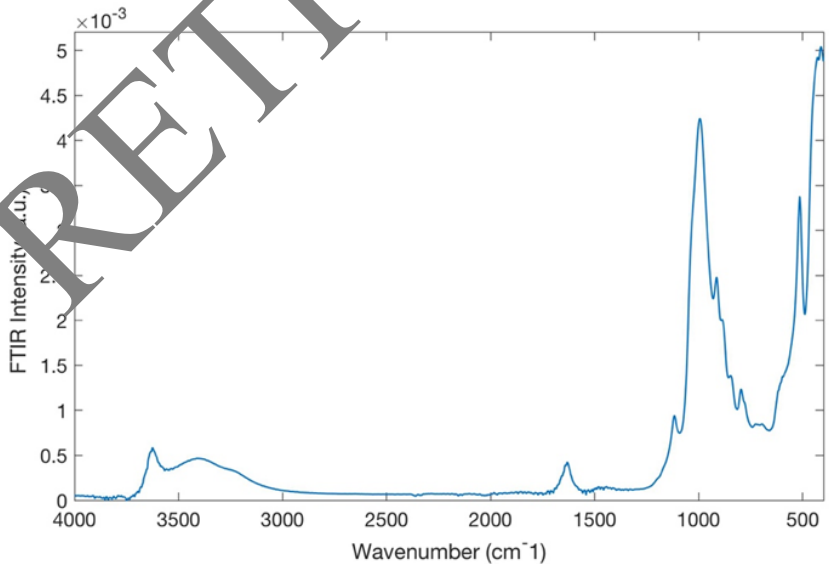

Figure 6. FTIR spectrum of montmorillonite in the resolution spectral range of 4000 ÷ 400 cm^{-1} at the temperature of T = 20 ℃.

The most significant peaks are located at ~ 3632 cm^{-1}, i.e. O-H stretching; at ~ 1639 cm^{-1} that represents the O-H bending (hydration); at ~ 1113 cm^{-1} and 1035 cm^{-1} make reference to the i-O stretching, out of plane and in plane, respectively. Finally, the peak at ~915 cm^{-1} denotes the AlAlOH bending, at ~793 cm^{-1} is situated the tridymite peak and the peak at ~529 cm^{-1} represents the Si-O bending vibration. Figure 7 shows the FTIR spectrum of BSA in the spectral range of 4000 ÷ 400 cm^{-1} at at the temperature of T = 20 ℃.

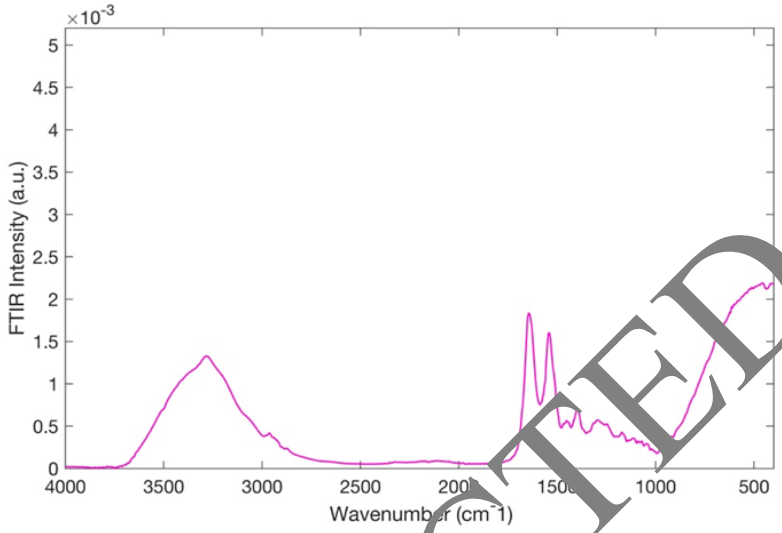

Figure 7. FTIR spectra of the BSA in the resolution spectral range of 4000 ÷ 400 cm^{-1} at temperature T = 20 ℃.

For the FTIR BSA spectrum, one of the most important IR spectral feature for the protein are the bands of Amide. In particular, in Figure 7 there are at ~ 3292 cm^{-1} the Amide A, at ~ 1649cm^{-1} Amide I and at ~ 1537cm^{-1} Amide II.

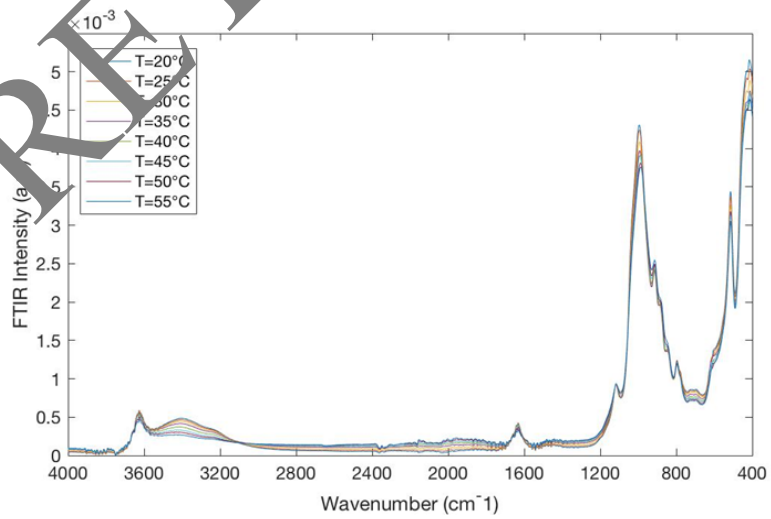

Figure 8. FTIR spectra for montmorillonite/water mixtures in the spectral range of 4000 ÷ 400 cm^{-1} and in the temperature range of 20 ℃ ÷ 55 ℃.

Figure 8 reports the FTIR spectra for montmorillonite/water mixtures in the spectral range of 4000 ÷ 400 cm^{-1} and in the temperature range of 20 ℃ ÷ 55 ℃. Figure 9 shows the FTIR spectra for montmorillonite/water mixtures/BSA in the spectral range of 4000 ÷ 400 cm^{-1} and in the temperature range of 20 ℃ ÷ 55 ℃.

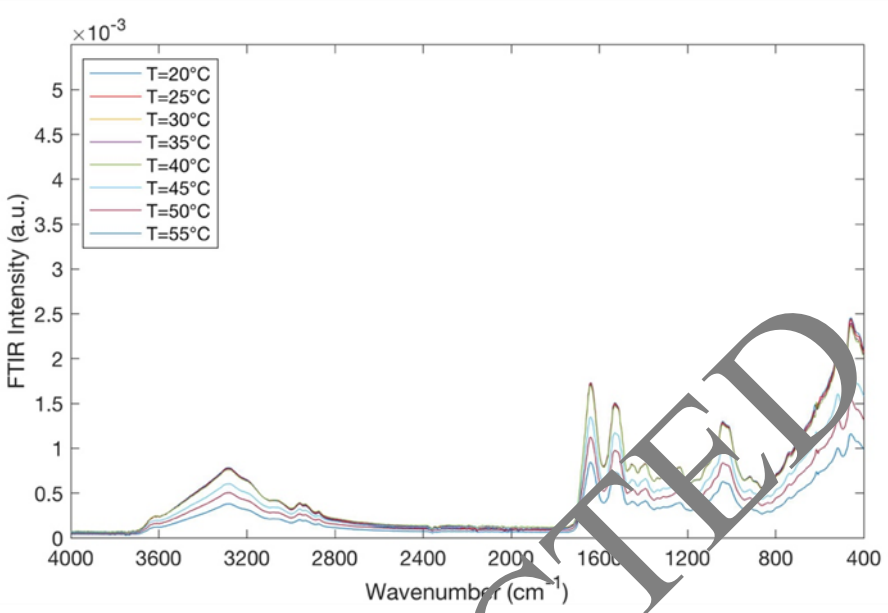

Figure 9. FTIR spectra for montmorillonite/water mixtures/BSA in the spectral range of 4000 ÷ 400 cm^{-1} and in the temperature range of 20 ℃ ÷ 55 ℃.

As it can be seen, in Figure 9, the typical IR bands of montmorillonite and the peaks of Bovine Serum Albumin (BSA) are observed. More precisely, by increasing temperature a little decrease in IR band intensity at ~ 3440 cm^{-1} of the O-H stretching band is observed; this suggests a dehydration of montmorillonite. The peaks at ~ 1649 and at 1537 cm^{-1} are typical of BSA and can be attributed to the C = O stretching vibration of the peptide linkages; they turn out to be very sensitive to the secondary structural components of the protein. These two peaks decrease with increasing temperature.

Before to proceed with the analysis of data, a pre-processing data procedure was performed by eliminating the background. To better investigate the mechanisms of interactions that occur between montmorillonite and BSA, the spectrum difference has been taken into account. In particular, from the spectrum of montmorillonite in the presence of BSA, the spectrum of montmorillonite has been subtracted the spectrum of montmorillonite so obtaining the spectrum difference. This procedure was adopted for each spectra of all the investigated temperatures. In Figure 10, the spectra differences, in the temperature range 20 ℃ ÷ 55 ℃, are reported.

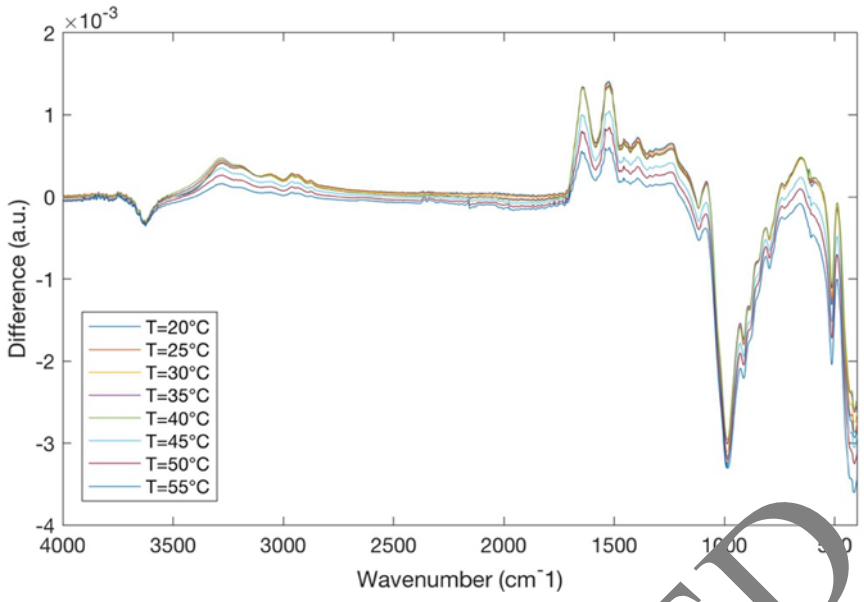

Figure 10. Spectra differences in the temperature range 20 ℃ ÷ 55 ℃.

The thermal behaviour of the investigated systems was characterized by the evaluation of SD (eq. 1). Figure 11 reports SD as a function of temperature for BSA (green circle) and for the spectrum difference (light blue square) together with their linear fits.

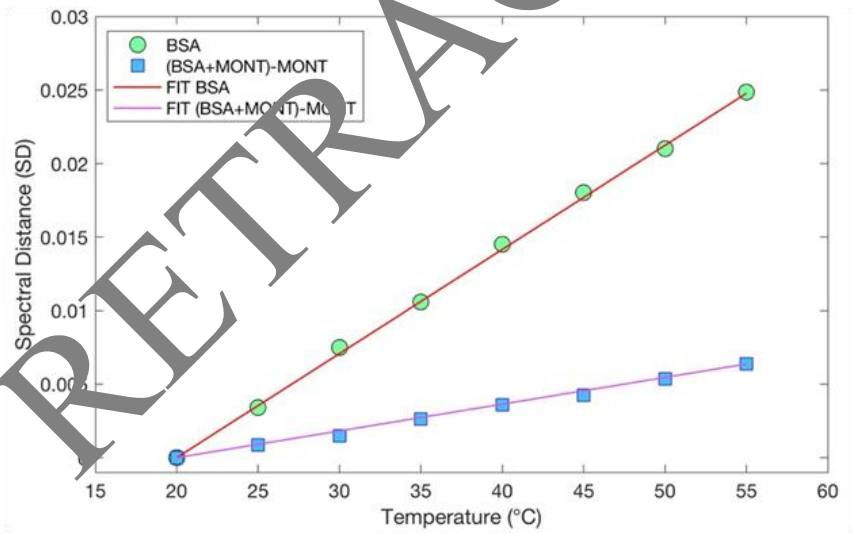

Figure 11. SD as a function of temperature for BSA (green circle) and for BSA in the presence of montmorillonite (light blue square) together with their linear fits (continuous lines).

In order to extract quantitative information, a linear fit has been performed:

$$y = ax + b \tag{2}$$

By this examination, it results that the slope coefficient value for the spectrum difference, $m = 1.82 \cdot 10^{-4}$, is lower than the slope coefficient value for BSA, that is equal to $m = 7.08 \cdot 10^{-4}$. This suggests that BSA in presence of montmorillonite has a higher thermal resistance and for this reason montmorillonite can be considered as an effective thermal bioprotector.

Another approach to investigate the thermal behavior of montmorillonite consists in applying the wavelet cross correlation method, that allows to determine, evaluating the wavelet cross-correlation coefficient, r_{XWT}, the degree of affinity between two signals. Such a method is very innovative and powerful and is employed in several kinds of disciplines such as climate, geoscience, physics, mathematics, finance, engineering science and others [115–120]. Let's consider two wavelet transforms, $W_1(s,\tau)$ and $W_2(s,\tau)$ of the investigated spectra, where s represents the scale parameter ($s > 0$)and τ denotes the shift parameter, and the two wavelet spectra $P_1(s)$ and $P_2(s)$ [121–125]. From a mathematical point of view $W(s,\tau)$is the inner product of the function $f(x)$ and scaled and shifted mother wavelets ψ:

$$w(a,\tau) = \frac{1}{a}\int_{-\infty}^{+\infty} f(x)\psi^*|x-\tau|\,dx;$$

where $f(x)$ denotes the one-dimensional function, * is the complex conjugate, and ψ is the mother wavelet:

$$\psi_{s,\tau} = \frac{\psi(x-\tau)}{\sqrt{s}}; \tag{3}$$

then, one defines the wavelet spectrum $P(s)$:

$$P(s) = \frac{1}{s}|w(s,\tau)|^2 dx; \tag{4}$$

and finally, one determines the wavelet cross-correlation coefficient, r_{XWT}:

$$r_{XWT}(s) = \frac{\int W_1(s,\tau)W_2^*(s,\tau)d\tau}{\sqrt{P_1(s)P_2(s)}} \tag{5}$$

The wavelet cross-correlation coefficient varies in the range $-1 \le r_{XWT} \le 1$; if the value is equal to 1 indicates a positive statistical relationship between the spectra; if the value is equal to 0 no statistical relationship between spectra exists; finally, if the value is equal to -1 a negative correlation between the two spectra is present. In the present study, the spectrum at lowest temperature (T = 20 ℃) has been chosen as reference wavelet spectrum both for BSA and for the spectrum difference.

Figure 12 shows the evaluated wavelet cross-correlation coefficient, r_{XWT}, versus temperature for BSA (orange circles) and for the spectrum difference (magenta squares) together with their linear fits.

What it emerges is that r_{XWT} decreases by increasing temperature following a decreasing linear trend. Also in this case, a linear fit has been performed and the slope coefficient value for the spectrum difference, $m = 0.8159$ is lower than the slope coefficient value for BSA, that is equal to

$m = 0.9245$. These results confirm that montmorillonite can be considered as a thermal bioprotector.

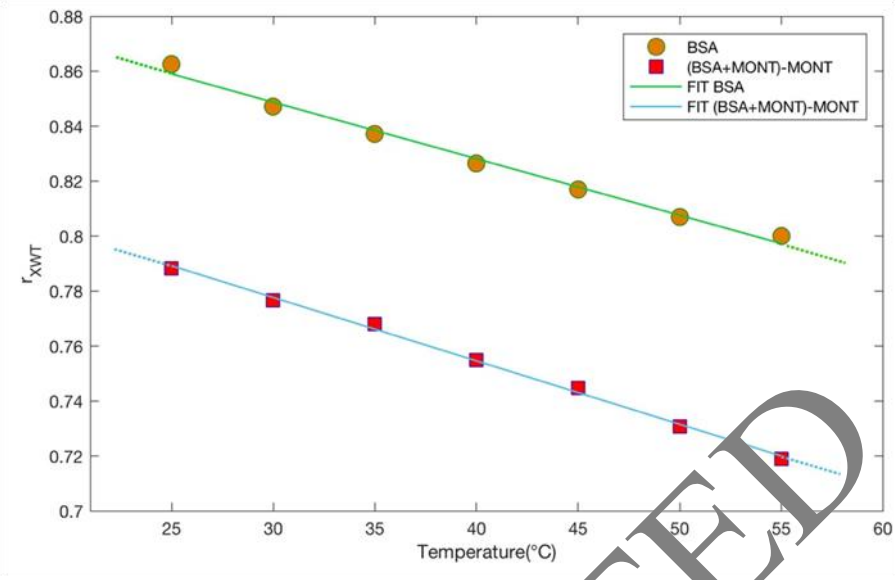

Figure 12. Wavelet cross-correlation coefficient, r_{XWT}, versus temperature together with their linear fits.

4. Conclusion

The present experimental work has allowed to show the importance of montmorillonite clay as a thermal bioprotector. FTIR data were collected to study the interaction of montmorillonite with BSA. SD and wavelet analyses, constitute two effective and innovative approaches for the characterization of the thermal properties of pure BSA and od BSA in the presence of montmorillonite. Both approaches suggest that BSA in the presence of montmorillonite has a lower spectral sensitivity when the temperature changes and, hence, the role of montmorillonite as a thermal bioprotector is thus justified. This is also evidenced by the theory widely discussed in the introduction of the paper regarding the birth of the first life forms on Earth in montmorillonite clay, in which the protective role of the montmorillonite interlayer space is also highlighted.

Acknowledgments (All sources of funding of the study must be disclosed)

This work is to be framed within the Progetto di Ricerca e Sviluppo ““Materiali di nuova generazione per il restauro dei Beni Culturali: nuovo approccio alla Fruizione (AGM for CuHe: Advanced Green Materials for Cultural Heritage)” Asse II “Sostegno all’innovazione”, Area di Specializzazione “Cultural Heritage” Avviso n. 1735/Ric del 13 luglio 2017 - Codice CUP B66G18000500005, codice identificativo Progetto ARS01_00697 nell’ambito del Programma Operativo Nazionale “Ricerca e Innovazione” 2014 - 2020 (PON R&I 2014 - 2020).

Conflict of interest

The authors declare that there is no conflict of interest regarding the publication of this article.

References

1. Leach S (2015) Origins of life. *Adv Chem Phys* 157: 293–313.
2. Haldane JBS (1929) The origin of life. *Rationalist Annual* 148: 3–10.
3. Bernal JD (1949) The physical basis of life. *P Phys Soc* 62: 597.
4. Cains-Smith AG (1982) *Genetic Takeover*. Cambridge: Cambridge University Press.
5. Lehn JM (2002) Toward complex matter: Supramolecular chemistry and self-organization. *PNAS* 99: 4763–4768.
6. Lehn JM (2002) Toward self-organization and complex matter. *Science* 295: 2400–2403.
7. Bada JL, Lazcano A (2003) Perceptions of science. Prebiotic soup-revisiting the Miller experiment. *Science* 300: 745–746.
8. Watson JD, Crick FHC (1953) Molecular structure of nucleic acids. *Nature* 171: 737–738.
9. Troland LT (1914) The chemical origin and regulation of life. *The Monist* 22: 92–133.
10. Muller HJ (1961) Genetic nucleic acid: Key material in the origin of life. *Persp Biol Med* 5: 1–23.
11. Gilbert W (1986) Origin of life: The RNA world. *Nature* 319: 618–618.
12. Hassen C (2015) Man creation had began since the creation of the first biological material very likely in clay. *Int J Mod Anthrop* 1: 49–65.
13. Luisi PL (2006) *The Emergence of Life: From Chemical Origins to Synthetic Biology.* Cambridge: Cambridge University Press.
14. Szostak JW, Bartel DP, Luisi PL (2001) Synthesizing life. *Nature* 409: 387–390.
15. Nielsen PE, Egholm M, Berg RH, et al. (1991) Sequence-selective recognition of DNA by strand displacement with a thymine-substituted polyamide. *Science* 254: 1497–1500.
16. Lazcano A (2010) Historical development of origins research. *Cold Spring Harbor Persp BioL* 2: a002089.
17. Wachtershauser G (1988) Before enzymes and templates, a theory of surface metabolism. *Microbiol Rev* 52: 452–484.
18. Haldane JBS (1954) The origins of life. *New Biol* 16: 12–27.
19. Muller HJ (1966) The gene material as the initiator and the organizing basis of life. *Am Naturalist* 100: 493–517.
20. Raven PH, Johnson GB, Mason KA, et al. (2014) The nature of molecules and properties of water. *Biology*, 10 Eds., New York: McGraw-Hill, 17–30.
21. Reece JB, Urry LA, Cain ML, et al. (2011). Water and life. *Campbell Biology,* 10 Eds., San Francisco: Pearson, 44–54.
22. Caetano-Anollés G, Wang M, Caetano-Anollés D (2013) Structural phylogenomics retrodicts the origin of the genetic code and uncovers the evolutionary impact of protein flexibility. *PLoS One* 8: e72225.
23. Eigen M, Lindemann BF, Tietze M, et al. (1989) How old is the genetic code? Statistical geometry of tRNA provides an answer. *Science* 244: 673–679.
24. Ertem G, Ferris JP (2000) Sequence and regio-selectivity in the montmorillonite catalyzed synthesis of RNA. *Orig Life Evo Biosph* 30: 411–422.

25. Farias ST, do Rego TG, José MV (2014). Evolution of transfer RNA and the origin of the translation system. *Fron Genet* 5 : 303–306.
26. Ghadiri M, Chrzanowski W, Rohanizadeh R (2015). Biomedical applications of cationic clay minerals. *RSC Adv* 5: 29467–29481.
27. de Paiva LB, Morales AR, Díaz FRV (2008) Organoclays: properties, preparation and applications. *App Clay Sci* 42: 8–24.
28. Datta M (2013) Clay–polymer nanocomposites as a novel drug carrier: Synthesis, characterization and controlled release study of Propranolol Hydrochloride. *Appl Clay Sci* 80–81: 85–92.
29. Xiang Y, Villemure G (1996) Electrodes modified with synthetic clay minerals: electrochemistry of cobalt smectites. *Clays Clay Miner* 44: 515–521.
30. Patel HA, Somani RS, Bajaj HC, et al. (2006) Nanoclays for polymer nanocomposites, paints, inks, greases and cosmetics formulations, drug delivery vehicle and waste water treatment. *Bull Mater Sci* 29: 133–145.
31. Yu WH, Li N, Tong DS, et al. (2013) Adsorption of proteins and nucleic acids on clay minerals and their interactions: A review. *Appl Clay Sci* 80–81: 443–452.
32. STĂNESCU VN, Olteanu M, Florea-Spiroiu M, et al. (2008) Fractal properties of collagen/chitosan/montmorillonite membranes. *Rev Roum Chim* 54: 767–771.
33. Raussell-Colom JA (1987) Reactions of clays with organic substances. *Chem Clays Clay Miner, Mineral Soc* 412–415.
34. Bergaya F, Lagaly G (2001) Surface modifications of clay minerals. *Appl Clay Sci* 19: 1–3.
35. Caccamo MT, Mavilia G, Mavilia L, et al. (2020) Self-assembly processes in hydrated montmorillonite by FTIR investigations. *Materials* 13: 1100.
36. Maina E, Wanyika H, Gachanja A (2016) Natural pyrethrum extracts photo-stabilized with organo clays. *J Sci Res Rep* 9: 1–20.
37. Ismadji S, Soetaredjo F, Ayucitra A, et al. (2015) Natural clay minerals as environmental cleaning agents. *J Clay Mat Environ Rem* 8: 3–37.
38. Celis R, HermosÍN C, Cornejo L, et al. (2010) Clay–herbicide complexes to retard picrolam leaching in soil. *Int J Environ Anal Chem* 82: 503–517.
39. Xi Y, Frost RL, He H (2007) Modification of the surfaces of Wyoming montmorillonite by the cationic surfactants alkyl trimethyl, dialkyl dimethyl and trialkylmethyl ammonium bromide. *J Coll Interf Sci* 305: 150–158.
40. Savelyev YV, Savchenko AN (2019) Exfoliation of montmorillonite in polymer matrix and its influence on the nanocomposites properties. *Polym J* 41: 149–158.
41. Emiel JM, Hensen SB (2002) Why clay swell. *J Phys Chem B* 106: 12664–12667.
42. Tyagi B, Chudasama CD, Jasra RV (2006) Determination of structural modification in acid activated montmorillonite clay by FT-IR spectroscopy. *Spectrochim Acta A* 64: 273–278.
43. Temuujin J, Jadambaa T, Burmaa G, et al. (2004) Characterisation of acid activated montmorillonite clay from tuulant (Mongolia). *Ceram Int* 30: 251–255.
44. Bonaccorsi L, Calandra P, Kiselev MA, et al. (2013) Self-assembly in poly(dimethylsiloxane)-poly(ethylene oxide) block copolymer template directed synthesis of linde type A zeolite. *Langmuir* 29: 7079–7086.
45. Bonaccorsi L, Calandra P, Amenitsch H, et al. (2013) Growth of fractal aggregates during template directed SAPO-34 zeolite formation. *Microporous Mesoporous Mat* 167: 3–9.
46. Bonaccorsi L, Lombardo D, Longo A, et al. (2009) Dendrimer template directed self-assembly during zeolite formation. *Macromol* 42: 1239–1243.

47. Chen C, Wylie RAL, Klinger D, et al. (2017) Shape control of soft nanoparticles and their assemblies. *Chem Mater* 29: 1918–1945.
48. Kiselev MA, Lombardo D (2017) Structural characterization in mixed lipid membrane systems by neutron and X-ray scattering. *Biochem Biophys Acta-Gen Sub* 1861: 3700–3717.
49. Lombardo D, Munaò G, Calandra P, et al. (2019) Evidence of pre-micellar aggregates in aqueous solution of amphiphilic PDMS–PEO block copolymer. *PCCP* 21: 11983–11991.
50. Rao Y, Blanton TN (2008) Polymer nanocomposites with a low thermal expansion coefficient. *Macromolecules* 41: 935–941.
51. Huang W, Ferris JP (2006) One-step, regioselective synthesis of up to 50-mers of RNA oligomers by montmorillonite catalysis. *J Am Chem Soc* 128: 8914–8919.
52. He H, Guo J, Xie X, et al. (2002) Microstructural study of acid-activated montmorillonite from Choushan, China. *Clay Miner* 37: 337–344.
53. Ferris JP (2005) Mineral calalysis and prebiotic synthesis: Montmorillonite-catalyzed formation of RNA. *Elements* 1: 145–149.
54. Joshi PC, Pitsch S, Ferris JP (2000) Homochiral selection in the montmorillonite-catalyzed and uncatalyzed prebiotic synthesis of RNA. *Chem Comm:* 2497–2498.
55. Mazo MA, Manevitch LI, Gusarova EB, et al. (2008) Molecular dynamics simulation of thermomechanical properties of montmorillonite crystal. 3. Montmorillonite crystals with PEO oligomer intercalates. *J Phys Chem B* 112: 3597–3604.
56. Adams JM (1987) Synthetic organic chemistry using pillared, cation-exchanged and acid- treated montmorillonite catalysts—A review. *Appl Clay Sci* 1987: 309–342.
57. Miyakawa S, Ferris JP (2003) Sequence-and regioselectivity in the montmorillonite-catalyzed synthesis of RNA. *J Am Chem Soc* 125: 8202–8208.
58. Kawamura K, Ferris JP (1999) Clay catalysis of oligonucleotide formation: kinetics of the reaction of the 5'-phosphorimidazolides of nucleotides with the non-basic heterocycles uracil and hypoxanthine. *Orig Life Evol Biosph* 29: 563–591.
59. Joshi PC, Aldersley MF, Delano JW, et al. (2009) Mechanism of montmorillonite catalysis in the formation of RNA oligomers. *J Am Chem Soc* 131: 13369–13374.
60. Knauth LP (1998) Salinity history of the earth's early ocean. *Nature* 395: 554–555.
61. Knauth LP (2005) Temperature and salinity history of the precambrian ocean: Implications for the course of microbial evolution. *Palaegeogr Palaeoclimatol Palacoecol* 2190: 53–69.
62. Hren MT, Tice MM, Chamberlain CP (2009) Oxygen and hydrogen isotope evidence for a temperature 3.42 billion years ago. *Nature* 462: 205–208.
63. Zhou ZJ, Cameron S, Kadatz B, et al. (1997) Clay swelling diagrams: their applications in formation damage control. *SPE J* 2: 99–106.
64. Sposito G (1984) *The Surface Chemistry of Soils*. New York: Oxford University Press, 115–2208.
65. Joshi PC, Aldersley MF, Delano JW, et al. (2009). Mechanism of montmorillonite catalysis in the formation of RNA oligomers. *J Am Chem Soc* 131: 13369–13374.
66. Hanczyc MM, Fujikawa SM, Szostak JW (2003) Experimental models of primitive cellular compartments: Encapsulation, growth, and division. *Science* 302*:* 618–622.
67. Hanczyc MM, Mansy SS, Szostak JW (2007) Mineral surface directed membrane assembly. *Orig Life Evol Biosph* 37: 67–82.
68. Mansy SS, Szostak JW (2008) Thermostability of model protocell membranes. *Proc Natl Acad Sci USA* 105: 3351–13355.
69. Guerrini L, Alvarez-Puebla RA, Pazos-Perez N (2018) Surface modifications of nanoparticles for stability in biological fluids. *Materials* 11: 1154.

70. Lombardo D (2009) Liquid-like ordering of negatively charged poly (amidoamine) (PAMAM) dendrimers in solution. *Langmuir* 25: 3271–3275.
71. Lombardo D (2014) Modeling dendrimers charge interaction in solution: Relevance in biosystems. *Biochem Res Int* 2014: 837651.
72. Lombardo D, Calandra P, Magazù S, et al. (2018) Soft nanoparticles charge expression within lipid membranes: The case of amino terminated dendrimers in bilayers vesicles. *Colloids Surf, B* 170: 609–616.
73. Hrenovic J, Milenkovic J, Ivankovic T, et al. (2012) Antibacterial activity of heavy metal-loaded natural zeolite. *J Hazard Mater* 201: 260–264.
74. Hu CH, Xu ZR, Xia MS (2005) Antibacterial effect of Cu^{2+}-exchanged montmorillonite on Aeromonas hydrophila and discussion on its mechanism. *Vet Microbiol* 109: 83–88.
75. Magana SM, Quintana P, Aguilar DH, et al. (2008) Antibacterial activity of montmorillonites modified with silver. *J Mol Catal A Chem* 281: 192–199.
76. Malachová K, Praus P, Rybková Z, et al. (2011) Antibacterial and antifungal activities of silver, copper and zinc montmorillonites. *Appl Clay Sci* 53: 642–645.
77. Morrison KD, Underwood JC, Metge DW, et al. (2014) Mineralogical variables that control the antibacterial effectiveness of a natural clay deposit. *Environ Geochem Health* 36: 613–631.
78. Tong G, Yulong M, Peng G, et al. (2005) Antibacterial effects of the Cu (II)-exchanged montmorillonite on Escherichia coli K88 and Salmonella choleraesuis. *Vet Microbiol* 105: 113–122.
79. Williams LB, Haydel SE (2010) Evaluation of the medicinal use of clay minerals as antibacterial agents. *Int Geol Rev* 52: 745–770.
80. Liyanapatirana C, Gwaltney SR, Xia K (2009) Transformation of triclosan by Fe (III)-saturated montmorillonite. *Environ Sci Technol* 44: 668–674.
81. Qin C, Troya D, Shang C, et al. (2014) Surface catalyzed oxidative oligomerization of 17 β -estradiol by Fe^{3+}-saturated montmorillonite. *Environ Sci Technol* 49: 956–964.
82. Qin C, Chen C, Shang C, et al. (2018) Fe^{3+}-saturated montmorillonite effectively deactivates bacteria in wastewater. *Sci Total Environ* 622–623: 88–95.
83. Majorek KA, Porebski PJ, Dayal A, et al. (2012) Structural and immunologic characterization of bovine, horse, and rabbit serum albumins. *Mol Imm* 52: 174–182.
84. Benkő M, Varga N, Bebők D, et al. (2015) Bovine serum albumin-sodium alkyl sulfates bioconjugates as drug delivery systems. *Coll Surf B Biointerf* 130: 126–132.
85. Xu W, Peng J, Ni D, et al. (2020) Preparation, characterization and application of levan/montmorillonite biocomposite and levan/BSA nanoparticle. *Carb Polym* 234: 115921.
86. Minutoli L, Altavilla D, Bitto A, et al. (2008) Trehalose: A biophysics approach to modulate the inflammatory response during endotoxic shock. *Eur J Pharm* 589: 272–280.
87. Maisano G, Majolino D, Migliardo P, et al. (1993) Sound velocity and hydration phenomena in aqueous polymeric solutions. *Mol Phys* 78: 421–435.
88. Magazù S, Migliardo F, Affouard F, et al. (2010) Study of the relaxational and vibrational dynamics of bioprotectant glass-forming mixtures by neutron scattering and molecular dynamics simulation. *J Chem Phys* 132: 184512.
89. Adamo A, Calabrò E, Magazù S (2019) Thermostabilization of BSA in TMAO water mixtures by infrared spectroscopy. *Curr Chem Biol* 13: 49–59.
90. Magazù S, Caccamo MT (2019) Study of trehalose effects on bsa solutions. In Łopieńska-Biernat E., Stryiński R., *Trehalose: Sources, Chemistry and Applications*, Hauppauge: Nova Science Publishers, 43–62.

91. Magazù S, Migliardo F, Benedetto A, et al. (2013) Protein dynamics by neutron scattering: The protein dynamical transition and the fragile-to-strong dynamical crossover in hydrated lysozyme. *Chem Phys* 424: 26–31.
92. Magazù S, Migliardo F, Benedetto A (2011) Puzzle of protein dynamical transition. *J Phys Chem B* 115: 7736–7743.
93. Fenimore PW, Frauenfelder H, Magazù S, et al. (2013) Concepts and problems in protein dynamics. *Chem Phys* 424: 2–6.
94. Magazù S, Calabro E, T Caccamo M, et al. (2016) The shielding action of disaccharides for typical proteins in aqueous solution against static, 50 Hz and 1800 MHz frequencies electromagnetic fields. *Curr Chem Biol* 10 : 57–64.
95. Magazù S, Migliardo F, Benedetto A, et al. (2013) Bioprotective effects of sucrose and trehalose on proteins. In Magazù, S., *Sucrose: Properties, Biosynthesis and Health Implications*, Hauppauge: Nova Science Publishers, 43–62.
96. Cannuli A, Caccamo MT, Magazù S (2018) Modeling and self organization dynamics of aggregation processes in acoustically levitated disaccharides solutions. *AAPP Atti della Accademia Peloritana dei Pericolanti, Classe di Scienze Fisiche, Matematiche e Naturali*, 96: 3.
97. Squire PG, Maser P, O'Konski CT (1968) The hydrodynamic properties of bovine serum albumin monomer and dimmer. *Biochem* 7: 4261–4272.
98. De Paz RA, Dale DA, Barnett CC, et al. (2002) Effects of drying methods and additives on the structure, function, and storage stability of subtilisin: role of protein conformation and molecular mobility. *Enzyme Microb Technol* 31: 765–774.
99. Xu Y, Hanna MA (2008) Morphological and structural properties of two-phase coaxial jet electrosprayed BSA-PLA capsules. *J Microencapsul* 25: 469–477.
100. Kopac T, Bozgeyik K, Yener J (2008) Effect of pH and temperature on the adsorption of bovine serum albumin onto titanium dioxide. *Coll Surf Physicochem Engin Aspects* 322: 19–28.
101. Yohannes G, Wiedmer SK, Elomaa M, et al. (2010) Thermal aggregation of bovine serum albumin studied by asymmetrical flow field-flow fractionation. *Anal Chim Acta* 675: 191–198.
102. Alkan M, Demirbas O, Doğan M, et al. (2006) Surface properties of bovine serum albumin—adsorbed oxides: Adsorption, adsorption kinetics and electrokinetic properties. *Micro Meso Materials* 96: 331–340.
103. Magazù S, Migliardo F, Benedetto A (2011) Elastic incoherent neutron scattering operating by varying instrumental energy resolution: Principle, simulations, and experiments of the resolution elastic neutron scattering (RENS). *Rev Sci Instr* 82: 105115.
104. Migliardo F, Magazù S, Caccamo MT (2013) Infrared, Raman and INS studies of poly-ethylene oxide oligomers. *J Mol Struc* 1048: 261–266.
105. Calabrò E, Condello S, Currò M, et al. (2013) Effects of low intensity static magnetic field on FTIR spectra and ROS production in SH-SY5Y neuronal-like cells. *Bioelectromagn* 34: 618–629.
106. Varga B, Migliardo F, Takacs E, et al. (2008) Neutron scattering studies on dUTPase complex in the presence of bioprotectant systems. *Chem Phys* 345: 250–258.
107. Cannuli A, Caccamo MT, Castorina G, et al. (2018) Laser techniques on acoustically levitated droplets. *EPJ Web of Confer* 167: 5010.
108. Egli M (2016) Diffraction techniques in structural biology. *Curr Protoc Nucleic Acid Chem* 65: 7.13.1–7.13.41.
109. Dong M, Husale S, Sahin O (2009) Determination of protein structural flexibility by microsecond force spectroscopy. *Nature nanotechn* 4: 514–517.

110. Becker W, Bhattiprolu KC, Gubensäk N, et al. (2018) Investigating protein-ligand interactions by solution nuclear magnetic resonance spectroscopy. *Chemphyschem: Eur J Chem Phys Phys Chem* 19: 895–906.
111. Magazù S, Maisano G, Migliardo F, et al. (2008) Elastic incoherent neutron scattering on systems of biophysical interest: Mean square displacement evaluation from self-distribution function. *J Phys Chem B* 112: 8936–8942.
112. Caccamo MT, Magazù S (2018) Applications of wavelet analyses on spectroscopic experiments. In: Burgess, J., *Wavelets: Principles, Analysis and Applications*, Hauppauge: Nova Science Publishers, 77–90.
113. Caccamo MT, Magazù S (2016) Tagging the oligomer-to-polymer crossover on EG and PEGs by infrared and Raman spectroscopies and by wavelet cross-correlation spectral analysis. *Vib Spectr* 85: 222–227.
114. Caccamo MT, Zammuto V, Gugliandolo C, et al. (2018) Thermal restraint of a bacterial exopolysaccharide of shallow vent origin. *Int J Biol Macromol* 114: 649–65
115. Magazù S, Calabrò E, Caccamo MT (2018) Experimental study of thermal restraint in bio-protectant disaccharides by FTIR spectroscopy. *Open Biotech J* 12: 123–133.
116. Magazù S, Migliardo F, Vertessy BG, et al. (2013) Investigations of homologous disaccharides by elastic incoherent neutron scattering and wavelet multiresolution analysis. *Chem Phys* 424: 56–61.
117. Migliardo F, Caccamo MT, Magazù S (2014) Thermal analysis on bioprotectant disaccharides by elastic incoherent neutron scattering. *Food Biophys* 9: 99–104.
118. Veleda D, Montagne R, Araujo M (2012) Cross wavelet bias corrected by normalizing scales. *J Atmos Ocean Technol* 29: 1401–1408.
119. Caccamo MT, Cannuli A, Magazù S (2018) Wavelet analysis of near-resonant series RLC circuit with time-dependent forcing frequency. *Eur J Phys* 39: 045702.
120. Migliardo F, Caccamo MT, Magazù S (2013) Elastic incoherent neutron scatterings wavevector and thermal analysis on glass-forming homologous disaccharides. *J Non-Cryst Solids* 378: 144–151.
121. Torrence C, Compo GP (1998) A practical guide to wavelet analysis. *Bull Am Meteorol Soc* 79: 61–78.
122. Grinsted A, Moore JC, Jevrejeva S (2004) Application of the cross wavelet transform and wavelet coherence to geophysical time series. *Nonlin Processes Geophys* 2004: 561–566.
123. Magazù S, Caccamo MT (2018) Fourier and wavelet analyses of climate data. In Magazù, S., *New Trends in Physics Education Research*; Hauppauge: Nova Science Publishers, 225–242.
124. Caccamo MT, Magazù S (2018) Variable length pendulum analyzed by a comparative Fourier and wavelet approach. *Rev Mex Fis E* 64: 81–86.
125. Colombo F, Magazù S, Caccamo MT (2018)Wavelet analysis as a tool for characterizing trends in climatic data, In: Burgess, J., *Wavelets: Principles, Analysis and Applications,* Hauppauge: Nova Science Publishers, 55–76.